

X-ray Luminosities of Optically-Selected Cataclysmic Variables and Application to the Galactic Ridge X-ray Emission

R. C. Reis^{1*}, P. J. Wheatley^{2†}, B. T. Gänsicke², & J. P. Osborne³

¹*Institute of Astronomy, Madingley Road, Cambridge, CB3 0HA*

²*Department of Physics, University of Warwick, Coventry, CV4 7AL*

³*University of Leicester, University Road, Leicester, LE1 7RH*

2 May 2018

ABSTRACT

By studying *Swift* X-ray spectra of an optically-selected, non-magnetic sample of nearby cataclysmic variables (CVs), we show that there is a population with X-ray luminosity much lower than accounted for in existing studies. We find an average 0.5–10.0 keV luminosity of $8 \times 10^{29} \text{ erg s}^{-1}$ which is an order of magnitude lower than observed in previous samples. Looking at the co-added X-ray spectrum of twenty CVs, we show that the spectral properties of this optically-selected, low X-ray luminosity sample – likely characteristic of the dominant population of CVs – resembles that of their brighter counterpart, as well as the X-ray emission originating in the Galactic ridge. It is argued that if the space density of CVs is greater than the current estimates, as it is indeed predicted by population synthesis models, then CVs can significantly contribute to the Galactic ridge emission.

Key words:

Stars: Cataclysmic Variables (CVs) - X-rays: GRXE

1 INTRODUCTION

The serendipitous detection in 1962 of an almost uniform Cosmic X-ray Background (CXB) is regarded as one of the first discoveries of extrasolar X-ray astronomy (Giacconi et al. 1962) and is thought to be mostly due to unresolved active galactic nuclei together with type Ia supernovae (e.g. Zdziarski 1996; Draper & Balantyne 2009; Moretti et al. 2009). A decade later the possibility of a Galactic component to the total measured CXB was suggested (Cooke, Griffiths & Pounds 1970). Ensuing observations showed that this Galactic component to the X-ray background is concentrated near the Galactic disk, covering a continuous ridge of width $\sim 10^\circ$ extending along the Galactic plane for tens of degrees – the Galactic Ridge X-ray Emission (GRXE, see e.g. Worrall et al. 1982; Warwick et al. 1985, 1988).

Numerous authors have modelled the GRXE spectrum as originating from two collisionally-ionised plasma components (e.g., Koyama et al. 1986, 1996; Kaneda et al. 1997): A soft component (kT ~ 0.8 keV) possibly produced by supernova shock waves (e.g. Kaneda et al. 1997) and a hard (kT ~ 8 keV) component whose origin is still a topic of much discussion. Several explanations for the nature of this hard component have been suggested, amongst them: i) a superposition of discrete, faint X-ray sources such as cataclysmic variables (Worrall et al. 1982; Revnivtsev et al. 2006a,

2009) or ii) originating from diffuse gas regions such as molecular clouds illuminated by X-rays from point sources (e.g. Murakami et al. 2000) or bombarded by low-energy cosmic-ray electrons (e.g. Yusef-Zadeh et al. 2002), and/or non-thermal processes in the interstellar medium (e.g. Dogiel et al. 2002). The apparent thermal spectrum of the GRXE (Koyama et al. 1986) implies an emitting plasma with temperature of a few keV. The energy density of this hypothetical plasma is over two orders of magnitude higher than that of normal interstellar matter and its temperature is too high for it to be gravitationally bound to the Galactic plane (Koyama et al. 1996). Furthermore Dogiel et al. (2002) showed that the energy required to replenish the outflowing plasma is as high as $10^{42} \text{ erg s}^{-1}$ which is equivalent to the release of kinetic energy from one supernova occurring every 30 years in the Galactic plane region. With an expected rate of 2–3 supernovae per century in the whole Galaxy (Tammann 1982), this leads to the unlikely requirement that all the energy associated with supernovae in the Galaxy goes into exclusively heating this hypothetical diffuse plasma.

The absence of a plausible heating mechanism to this hypothetical diffuse thermal plasma, and the similarities of the X-ray spectra of the ridge and CVs, led many to believe that the ridge emission is still most likely to arise from as yet unresolved sources such as cataclysmic variables (CVs) and other accreting binary systems (Muno et al. 2004; Revnivtsev et al. 2007). An ultra-deep (1 Ms) Chandra ACIS-I study of the Galactic centre region (Revnivtsev et al. 2009) has successfully resolved over 80 percent of the diffuse emission into discrete sources at 6–7 keV (see also

* E-mail: rdsreis@umich.edu

† E-mail: p.j.wheatley@warwick.ac.uk

Hong 2012; Yuasa et al. 2012), however the nature of these sources remains uncertain (e.g. Warwick et al. 2011) and the contribution of CVs to the total GRXE luminosity function is still known. A key uncertainty is the X-ray luminosity function of CVs. Previous studies were suggestive of mean CV X-ray luminosities of $\log(< L_x >) \sim 31.5$ (Mukai & Shiokawa 1993; Verbunt et al. 1997) in the hard band (2.0–10.0 keV), with at least an order of magnitude spread about this mean value. Work done on *ASCA* data (Yamauchi et al. 1996) concluded that for CVs to be accountable for the GRXE the sources' 2.0–10.0 keV luminosity could not be higher than $2 \times 10^{33} \text{ erg s}^{-1}$. Based on model calculations, Tanaka et al. (1999) showed that the ridge emission requires a class of hard sources with a luminosity in the $10^{29-30} \text{ erg s}^{-1}$ range, thus making CVs apparently too luminous as a class.

Sazonov et al. (2006) found CVs contributing only at $L_x \gtrsim 10^{31} \text{ erg s}^{-1}$, but their sample was X-ray selected and were mostly consistent of magnetic CVs, and thus biased to high X-ray luminosities. On the other hand, a more recent study by Byckling et al. (2010) used a distance-limited sample of non-magnetic CVs with known distances and found systematically low luminosities concentrated around $L_x \approx 10^{30.5} \text{ erg s}^{-1}$. However, even this sample was biased to high accretion rates by reliance on inhomogeneous selection criteria such as dwarf nova outburst.

Until recently, the population of known CVs has been dominated by systems discovered because they displayed copious accretion activity, either in the form of outbursts, or X-ray emission (Gänsicke et al. 2002, 2005a). In contrast to this, population synthesis models have long predicted that the CV population should be dominated (>95%) by short-period low-luminosity systems with extremely low-mass donor stars (Kolb 1993; Howell et al. 2001) and thus should have average X-ray luminosities $\lesssim 10^{30} \text{ erg s}^{-1}$. Over the past years, the Sloan Digital Sky Survey (SDSS) has identified a substantial number of CVs whose optical spectra are dominated by a cool white dwarf (e.g. Szkody et al. 2009), implying very low secular average accretion rates (Townsend & Bildsten 2003; Townsend & Gänsicke 2009; Gänsicke et al. 2009), and that have extremely low-mass donor stars (Littlefair et al. 2006b, 2008). This sample of optically-selected, non-magnetic CVs provide the means to measure the X-ray luminosity of CVs towards the low-end of their luminosity function and thus to better assess their contribution to the Galactic ridge X-ray emission.

In the following sections we present results on *Swift*-XRT observations made on a sample of 20 CVs whose optical spectra are dominated by the white dwarf, indicative of low accretion rates. These are the systems expected to dominate in numbers the population of CVs.

2 TARGET SAMPLE

The Sloan Digital Sky Survey (SDSS; York et al. 2000) is an imaging and spectroscopic survey of the high Galactic latitude sky visible from the Northern hemisphere. We based our target selection on Data Release 5 (DR5), which covered over 8,000 deg^2 of the sky and performed spectroscopy on over 1 million objects (Adelman-McCarthy et al. 2006). Although the principle goal of this survey is to survey the large-scale distribution of galaxies and quasars, it has also provided vast amount of data on stars. Due to CVs having non-stellar colours they are serendipitously discovered by SDSS. Szkody et al. (2011) have identified close to 300 CVs, of which ~ 45 have a very low mass accretion rate and are thus dominated by the white dwarf.

For the *Swift* survey presented here, we selected 16 CVs from SDSS DR5 in which the optical spectrum is dominated by emission from a cool white dwarf. These spectra have been sky subtracted, corrected for telluric absorption and spectrophotometrically calibrated by the Spectro2d pipeline (Stoughton et al. 2002). This sample was supplemented by four additional low-mass transfer systems with similar optical properties: V455 And (Araujo-Betancor et al. 2005), PQ And (Schwarz et al. 2004; Patterson et al. 2005a), REJ1255+266 (Watson et al. 1996; Wheatley et al. 2000a; Patterson et al. 2005c) and ASAS0025+1217 (aka FL Psc, Templeton et al. 2006; Ishioka et al. 2007). The object names and coordinates of the 20 *Swift* targets are listed in Table 1. Our targets form a representative sample of spectroscopically selected low-luminosity CVs with distances in the range $\sim 75 - 400 \text{ pc}$ (see Sect. 4.1).

3 OBSERVATIONS AND DATA REDUCTION

Our sample of 20 optically-selected, non-magnetic CVs were observed using the X-Ray Telescope, XRT (0.2–10.0 keV) on board the *Swift* Gamma-Ray Burst Explorer (Gehrels et al. 2004). The various observations, listed in Table 1, were reduced using the tools provided in the HEASOFT v 6.9 software package. All data were extracted in the photon counting (PC) mode with the standard grade selection (0–12) for this mode. For each observation an image in the 0.2–10.0 keV band was obtained from which a spectrum was extracted from a circular region of radius $47''$, corresponding to 90 percent of the point spread function at 1.5 keV. Background spectra were extracted from an annular region centred on the X-ray source of inner and outer radius of $50''$ and $200''$ respectively. Response files (version 10) were downloaded¹ and used for spectral analysis. When looking at the spectrum of each individual target we used the ftool² GRPPHA to provide a minimum of 4 counts per bin and thus provide two or more independent spectral bins. Following this requirement only sources with 8 or more counts were individually analysed in this manner. Model fits were minimised using Cash statistics (C-stat in XSPEC; Cash 1979) due to the low number of counts per bin. All spectral analyses were performed using XSPEC v 12.7.0 (Arnaud 1996).

The source and background event files were used to calculate count-rates, R , for each target in the 0.5–10.0 keV energy band. The net counts were computed from the total counts in the source region less the background count, scaled by the ratio of the source/background area. The count-rate for each individual target was computed using the total live-time and the uncertainties are assumed to follow simple Poisson statistics. Table 1 list the net counts for the various observations. In order to analyse the sample as a group, in Sect. 4.2 we co-added all the individual spectra using the ftool XSELECT. For the co-added spectrum, a minimum of 20 counts per bin were used and model fits were minimised using χ^2 statistics.

¹ <http://heasarc.nasa.gov/docs/heasarc/caldb/data/swift/xrt/index.html>

² <http://heasarc.gsfc.nasa.gov/ftools/>

Table 1. System properties

Target	RA(2000)	Dec(2000)	P_{orb}	g	Live	Counts	Model Flux ^a	Distance ^b	Distance ^c	Luminosity	References
			(min)	mag.	time (s)	[0.5–10 keV]	$\times 10^{-13}$ erg cm ⁻² s ⁻¹	(pc)	(pc)	[0.5–10.0 keV] $\times 10^{29}$ (erg s ⁻¹)	
SDSS0131-0901	01 31 32.39	-09 01 22.3	81.5	18.3	4940	23.9	2.0 ± 0.5	240	219 ± 72	13.8 ± 6.4	1
SDSS0137-0912	01 37 01.06	-09 12 34.9	79.7	18.7	4493	16.2	1.5 ± 0.4	230	263 ± 86	9.4 ± 4.6	2
SDSS0843+2751	08 43 03.99	+27 51 49.7	85.5	18.9	476	$< 1^d$	< 0.3	240	288 ± 95	< 1.8	3,4
SDSS0904+0355	09 04 03.48	+03 55 01.2	86.0	19.3	5670	16.8	1.2 ± 0.3	260	347 ± 114	9.9 ± 4.8	5
SDSS0904+4402	09 04 52.09	+44 02 55.4		19.4	4367	1.0	0.09 ± 0.01	320	363 ± 119	1.2 ± 0.5	6
SDSS0919+0857	09 19 45.11	+08 57 10.0	81.3	18.2	167	$< 1^d$	< 2	220	209 ± 69	< 11	6,7
SDSS1137+0148	11 37 22.25	+01 48 58.6	109.6	18.7	3798	11.8	1.3 ± 0.4	220	263 ± 86	7.4 ± 0.4	8
SDSS1238-0339	12 38 13.73	-03 39 33.0	80.5	17.8	4106	40.3	4.1 ± 0.8	180	174 ± 57	15.7 ± 7.0	9
SDSS1339+4847	13 39 47.12	+48 47 27.5	82.5	17.7	4051	16.7	1.7 ± 0.5	170	166 ± 54	5.9 ± 2.8	10
SDSS1457+5148	14 57 58.21	+51 48 07.9	77.92	19.6	6293	14.8	1.0 ± 0.3	320	398 ± 131	11.9 ± 5.8	11
SDSS1501+5501	15 01 37.22	+55 01 23.4	81.9	19.4	4800	11.6	1.0 ± 0.3	300	363 ± 119	10.7 ± 5.5	12
SDSS1507+5230	15 07 22.33	+52 30 39.8	66.6	18.3	7002	15.6	0.9 ± 0.3	225	219 ± 72	5.6 ± 2.7	12,13,14
SDSS1556-0009	15 56 44.24	-00 09 50.2	106.7	18.0	7463	42.8	2.4 ± 0.4	135	191 ± 63	5.2 ± 2.3	7,15
SDSS1610-0102	16 10 33.64	-01 02 23.3	80.5	19.0	9400	18.8	0.8 ± 0.2	240	302 ± 99	5.7 ± 2.7	16,17
SDSS1702+3229	17 02 13.26	+32 29 54.1	144.1	17.9	6840	25.7	1.5 ± 0.4	180	-	6.0 ± 2.8	18,19
SDSS2048-0610	20 48 17.85	-06 10 44.8	87.3	19.4	14734	68.6	1.9 ± 0.3	270	363 ± 119	16.8 ± 7.3	20,21
ASAS0025+1217	00 25 11.07	+12 17 12.1	$\simeq 80$	17.4 ^v	3309	53.8	6.7 ± 1.2	125	145 ± 47	12.6 ± 5.5	22,23
PQ AND	02 29 29.54	+40 02 40.2	$\simeq 80$	19.0 ^v	13215	16.5	0.5 ± 0.1	150 ± 50	302 ± 99	1.4 ± 1.0	24,25
RE1255+266	12 55 10.56	+26 42 26.9	$\simeq 120?$	19.2	4298	8.8	0.8 ± 0.3	180 ± 50	326 ± 107	3.3 ± 2.2	26,27
V455 And	23 34 01.45	+39 21 41.0	81.1	16.5 ^v	8666	16.0	0.8 ± 0.2	90 ± 15	95 ± 31	0.7 ± 0.3	28

Notes: ^a Fluxes were calculated assuming the flux–count rate relationship given in the text (see Sect. 4.3.1) in the 0.5–10 keV range. ^b distances obtained by modelling the optical SDSS spectra, as described in the Sect. 4.1, with uncertainties of 20%, except for the last four targets, where published distance estimates are given. The distances listed in this column are used in the X-ray analysis. ^c distances obtained from $< M_g > = 11.6 \pm 0.7$ (Gaensicke et al. 2009), except for SDSS 1702+3229, whose period is too long to adopt this absolute magnitude. ^v V-band magnitude. ^d 1σ upper limit. **References:** ¹ Southworth et al. (2007); ² Pretorius et al. (2004); ³ Patterson et al. (1998); ⁴ Kato et al. (2004); ⁵ Woudt et al. (2005); ⁶ Dillon et al. (2008); ⁷ Thorstensen et al. in prep; ⁸ Patterson et al. (2003); ⁹ Zharikov et al. (2006); ¹⁰ Gänsicke et al. (2006b); ¹¹ Uthas et al. (2012); ¹² Littlefair et al. (2008); ¹³ Littlefair et al. (2007); ¹⁴ Patterson et al. (2008); ¹⁵ Woudt et al. (2004); ¹⁶ Woudt & Warner (2004); ¹⁷ Copperwheat et al. (2009); ¹⁸ Littlefair et al. (2006a); ¹⁹ Boyd et al. (2006); ²⁰ Woudt et al. (2005); ²¹ Dillon et al. in prep; ²² Templeton et al. (2006); ²³ Ishioka et al. (2007); ²⁴ Patterson et al. (2005b); ²⁵ Vanlandingham et al. (2005); ²⁶ Wheatley et al. (2000b); ²⁷ Patterson et al. (2005d); ²⁸ Araujo-Betancor et al. (2005)

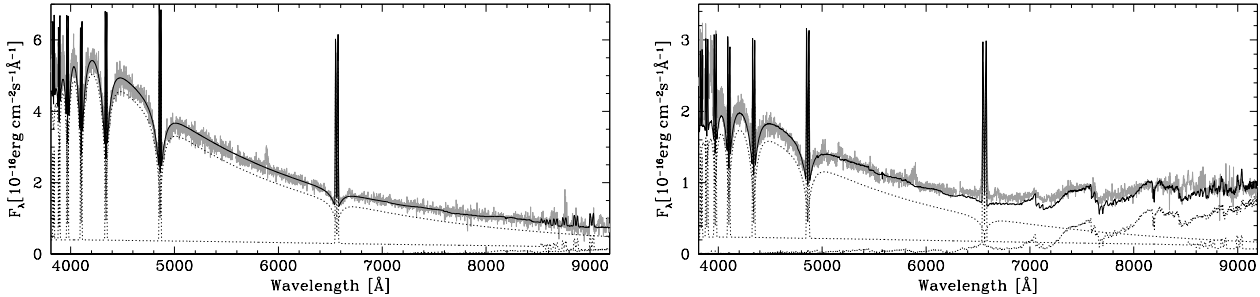


Figure 1. Three components model (white dwarf, optically thin disc, secondary star) of the average optical spectrum of SDSS 1339+4842 (left, Sp(2)=M8, $T_{\text{wd}} = 12500$ K, $T_{\text{d}} = 6500$ K, $\Sigma_{\text{d}} = 1.7 \times 10^{-2}$ g cm⁻² and $d = 170$ pc) and SDSS 1137+0148 (right, Sp(2)=M6.5, $T_{\text{wd}} = 13000$ K, $T_{\text{d}} = 6500$ K, $\Sigma_{\text{d}} = 3.5 \times 10^{-2}$ g cm⁻² and $d = 220$ pc). The observed data are shown in grey, the individual three components as dotted black lines, and the summed model as solid black line.

4 ANALYSIS AND RESULTS

4.1 Distance estimates

In order to calculate the luminosity distribution of the sample it was necessary to obtain an approximate distance to each individual source. This was done following two different approaches.

The first method consists of fitting a three-component model accounting for the flux contributions of the white dwarf, the accretion disc, and the companion star to the optical spectra of the 16 CVs for which SDSS spectroscopy is available. A detailed description of this approach can be found in Gänsicke et al.

(1997, 1999, 2006b), here we provide only a brief summary. The white dwarf is represented by model spectra computed with the TLUSTY/SYNPEC codes of Lanz & Hubeny (1995), with a fixed radius $R_{\text{wd}} = 8.7 \times 10^8$ cm implied by the Hamada & Salpeter (1961) mass-radius relation for an assumed mass of $M_{\text{wd}} = 0.6 M_{\odot}$. The secondary star is represented by observed templates covering spectral types (Sp(2)) M0.5 to M9 from Beuermann et al. (1998) and L0 to L8 from Kirkpatrick et al. (2000, 1999). The radius of the secondary star is estimated from Roche-lobe geometry, and depends primarily on the orbital period. Orbital period measurements are available for most of the targets (Ta-

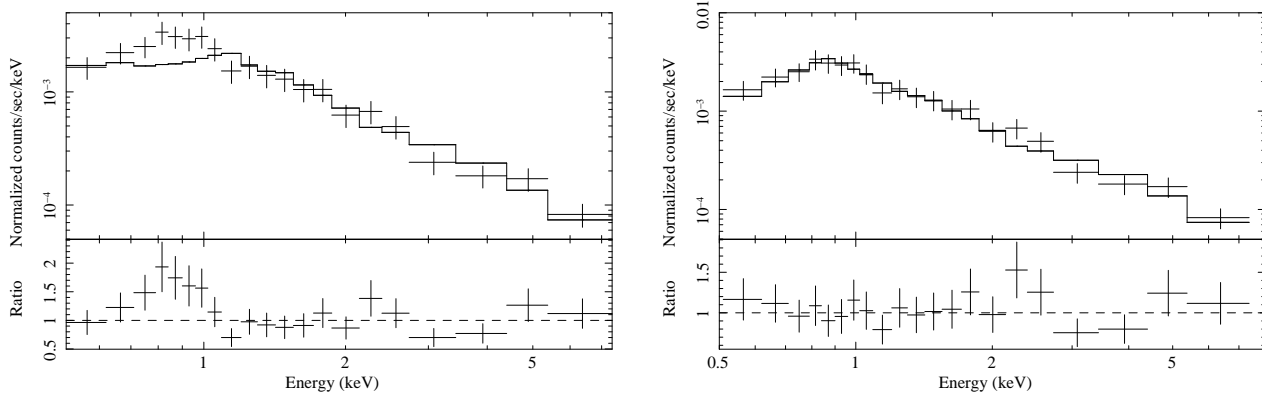


Figure 2. *Swift*-XRT X-ray background subtracted spectrum of combined sources. *Left:* Data/model of simple one-temperature thermal plasma with a temperature of ~ 6 keV. This model provided a poor fit with $\chi^2/\nu = 31.3/19$ and exhibited residual at energies $\lesssim 1.2$ keV. *Right:* Data/model ratio for two-temperature thermal plasma with temperatures of 8_{-3}^{+10} and $0.62_{-0.24}^{+0.16}$ keV as well as photoelectric absorption. This provided the best fit ($\chi^2/\nu = 11.3/17$) for the combined data.

ble 1), and it is apparent that most of the systems are located close to the 80 min period minimum, for which we adopt $R_2 = 8.6 \times 10^9$ cm. For SDSS 1137+0148 (RZ Leo), SDSS 1556-0009, and SDSS 1702+3229, we assume 1.28×10^{10} cm, 1.17×10^{10} cm, and 1.53×10^{10} cm, respectively. Free parameters in the three-component model are the white dwarf temperature T_{wd} , the distance d , the temperature T_d and column density Σ_d of the disk, as well as the spectral type of the secondary star. The parameters were varied in a forward-modelling approach until all three spectral components in the observed spectrum were consistently reproduced, Fig. 1 shows two example fits (SDSS 1137+0148 and SDSS 1337+0148), and Table 1 lists the distances determined by these fits. The uncertainty of the distances determined in this way is estimated to be $\simeq 20\%$ (see Howell et al. 2002; Szkody et al. 2002; Gänsicke et al. 2005b, 2006a,b, for a detailed description of the method employed here and associated uncertainties.).

Four of our targets have no SDSS spectrum, and Table 1 lists previously published distance estimates and references.

As a second method of estimating the distances to our targets we adopted the mean absolute magnitude for short-period CVs with white dwarf dominated spectra, $\langle M_g \rangle = 11.6 \pm 0.7$, which Gänsicke et al. (2009) established largely based on systems for which ultraviolet spectroscopy is available, and which leads to a $\sim 30\%$ uncertainty in the distance. The distances corresponding to the observed g and V magnitudes are also listed in Table 1, with the exception of SDSS 1702+3229, whose orbital period is too long to qualify for this method. For all systems, both distance estimates agree within the quoted errors. We note that an independent analysis of HST spectroscopy of SDSS1507+5230 led to a distance estimate of 250 ± 50 pc, (Uthas et al. 2011) entirely consistent with both of our own values (Table 1).

For the determination of the X-ray luminosities carried out in §4.3, we adopted the distances based on our three-component model for the 16 systems with SDSS spectra, and the published distances for the remaining four systems.

4.2 Spectral analysis

In order to investigate the spectral nature of the twenty optically selected CVs we co-added their individual spectra using the ftool XSELECT. The combined spectrum was then grouped so as to provide a minimum of twenty counts per energy bin and thus enable the use of χ^2 statistics. Figure 2 (*left*) shows the average spectrum fitted with a simple one-temperature thermal plasma model

(MEKAL model in XSPEC; Mewe et al. 1986; Liedahl et al. 1995) having a temperature of ≈ 6 keV (Model 1; Table 2). This model provides a poor fit with $\chi^2/\nu = 31.3/19$ and exhibited residual at energies $\lesssim 1$ keV. A much improved fit was achieved by the addition of a second thermal plasma model (in a similar manner to e.g. van Teeseling & Verbunt 1994; Wheatley et al. 1996) absorbed by a neutral hydrogen column (WABS³; Model 2, Fig. 2, *right*), however, it was found that the value of N_H is degenerate with the plasma temperature. Nonetheless, for a typical value of $N_H = 4 \times 10^{20} \text{ cm}^{-2}$ (Baskill et al. 2005), we find a temperature of $0.62_{-0.24}^{+0.16}$ keV, consistent with the values found by Baskill et al. (2005) for a sample of 34 CVs using a similar model. We have thus fixed the value of N_H to $4 \times 10^{20} \text{ cm}^{-2}$ when estimating the errors presented in Table 2.

The best fitting model for this sample of low-luminosity CVs is here interpreted as a two collisionally-ionised plasma with temperatures of 8_{-3}^{+10} and $0.62_{-0.24}^{+0.16}$ keV. Of course, the fact that we have two temperatures does not necessarily imply the presence of two discrete components in the X-ray spectrum as this likely a simple approximation to common cooling flow models which successfully represent the spectra of more luminous CVs (e.g. Wheatley et al. 1996; Mukai et al. 2003; Baskill et al. 2005; Byckling et al. 2010). The results presented here for the spectral properties of our sample of non-magnetic, low luminosity CVs are again consistent with that of the Galactic ridge emission (e.g. Koyama et al. 1986; Kaneda et al. 1997). Using the best-fit model, a count-rate of $4.0 \pm 0.2 \times 10^{-3} \text{ s}^{-1}$ resulted in a 0.5–10 keV unabsorbed energy flux⁴ of $1.6 \pm 0.2 \times 10^{-13} \text{ erg cm}^{-2} \text{ s}^{-1}$. These values were used as conversion factors between the 0.5–10 keV count rate and flux in the following section. We note here that for the only object common in both our sample and that of Byckling et al. (2010) (namely ASAS0025+12), the luminosity found here of $L_{0.5-10} = (1.3 \pm 0.6) \times 10^{30} \text{ erg s}^{-1}$ (Table 1), based on the methodology described above, is fully consistent with the value of $L_{2-10} = (1.6_{-0.8}^{+3.8}) \times 10^{30} \text{ erg s}^{-1}$ found in their work, even when considering the different energy range used in this work.

³ Using the standard BCMC cross-sections (Balucinska-Church & McCammon 1992) and ANGR abundances (Anders & Grevesse 1989).

⁴ Unabsorbed flux obtained using the XSPEC model CFLUX convolved with Model 2 from Table 2.

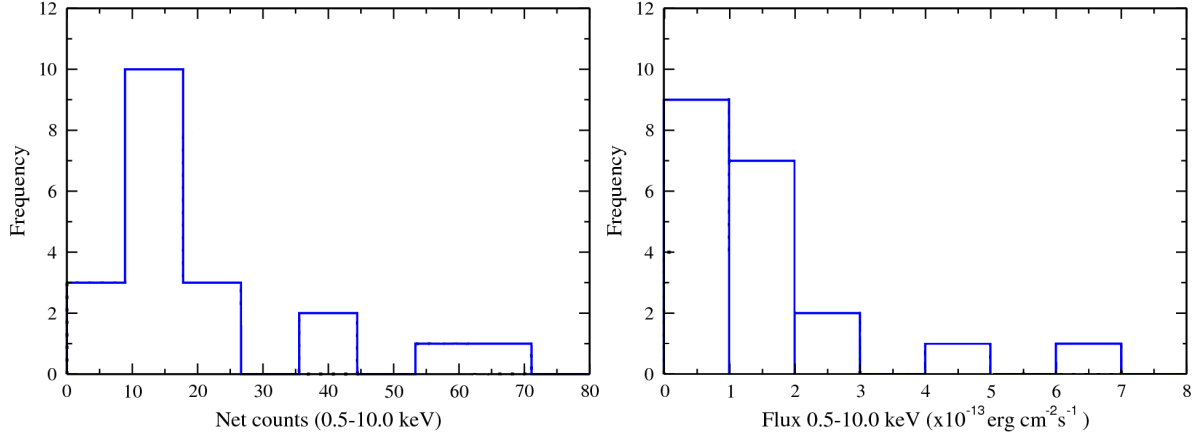


Figure 3. *Left:* Histogram of counts detected in the energy band 0.5–10.0 keV. *Right:* Same as before but for the flux obtained using the rate–flux conversion factor as described in Sect. 4.3.1.

Table 2. Model parameters for the combined source spectra.

Parameter	Model 1	Model 2
N_H ($\times 10^{20} \text{ cm}^{-2}$)	–	4
kT_1 keV	$5.8^{+2.0}_{-1.2}$	8^{+10}_{-3}
$Norm_1$ ($\times 10^{-5}$)	$8.2^{+0.8}_{-0.7}$	7.2 ± 0.8
kT_2 keV	–	$0.62^{+0.16}_{-0.24}$
$Norm_2$ ($\times 10^{-5}$)	–	0.8 ± 0.3
χ^2/ν	31.3/19	11.3/17

Notes— Model 1 is the single-temperature thermal plasma model MEKAL in XSPEC. Model 2 assumes a two-temperature thermal plasma with photoelectric absorption (WABS(MEKAL+MEKAL) in XSPEC). The value of N_H was frozen at $4 \times 10^{20} \text{ cm}^{-2}$. The quoted error corresponds to a 90 per cent confidence level for one parameter of interest ($\Delta\chi^2 = 2.71$).

4.3 X-ray photometry

4.3.1 Energy fluxes

A histogram of the number of sources as a function of the counts in the 0.5–10.0 keV energy range is shown in Fig. 3 (*Left*). In order to obtain an estimate of the energy flux (in $\text{erg cm}^{-2} \text{ s}^{-1}$) we used the spectral model described in the previous section to compute an average conversion factor between count-rate (R) and energy flux in the range 0.5 – 10 keV. We find (Sect. 4.2) that for the combined spectrum of all twenty sources, a two-temperature optically thin plasma model absorbed by a neutral hydrogen column equivalent to $N_H \approx 4 \times 10^{20} \text{ cm}^{-2}$ yields a conversion factor for the unabsorbed energy flux of $F_{(0.5-10)} = (4.1 \pm 0.4) \times 10^{-11} \times R \text{ erg cm}^{-2} \text{ s}^{-1}$, where R is the count-rate in the 0.5–10 keV energy band. As a consistency check we used this model to fit the individual spectra of the 4 observations with over 40 counts (see Table 2) allowing only a multiplicative constant to vary. This resulted in values for the conversion factor varying from approximately 3.8 to 4.6×10^{-11} , in agreement with the value above. The fluxes for the various targets obtained as described are also listed in Table 1 and shown in Fig. 3 (*Right*).

4.3.2 Luminosity distribution

Table 1 lists the calculated 0.5–10.0 keV luminosities of all twenty sources. The large error in these values are the result of propagated errors in both the distance and flux. A histogram of the number of sources as a function of log-luminosity is displayed in Fig. 4.

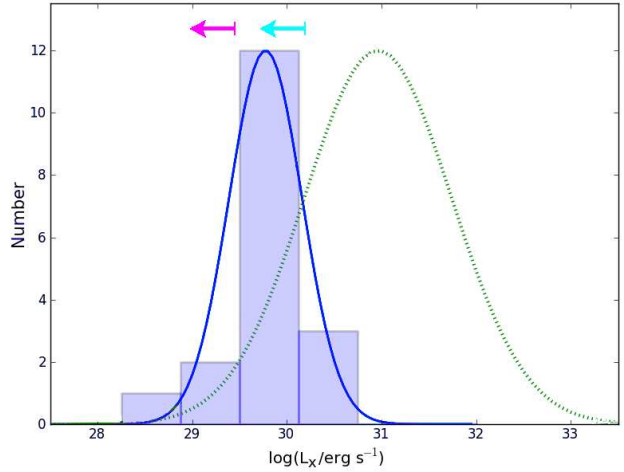


Figure 4. X-ray luminosity distribution for a sample of optically-selected CVs (blue). Only sources with observed fluxes consistently greater than zero are included in the histogram. The magenta and cyan arrows shows the upper limits for SDSS0843+2751 and SDSS0919+0857 respectively. The mean Gaussian distribution (solid blue) has $\langle \log(L_{0.5-10}) \rangle = 29.78$ with a variance of 0.16. For comparison with previous, X-ray selected surveys, we show in green the (renormalised) Gaussian distribution obtained for the 46 sources catalogued by the *ROSAT* all sky survey (derived from Verbunt et al. 1997 scaled to the 0.5–10 keV range used in this work. This illustrative, X-ray selected, distribution has a mean value of $\langle \log(L_{2-10}) \rangle = 30.96$ and a variance of 0.78, clearly higher than our sample.

SDSS0843+2751 and SDSS0919+0857 were not used in the construction of the histogram due the sources having a count rate consistent with zero, possibly resulting from their short exposure time (see Table 1). However the upper limits to their luminosities are displayed with magenta and cyan arrows respectively. The solid red line shows the Gaussian distribution for the mean (0.5–10 keV) log-luminosity with $\langle \log(L_{0.5-10}) \rangle = 29.78$ and a variance of 0.16. For comparison, in Fig. 4 we show in green the (renormalised) luminosity distribution obtained from the X-ray selected *ROSAT* all sky survey catalogue from Verbunt et al. (1997) after scaling to the 0.5–10 keV range used here assuming Model 2 (outlined in Table 2 and described in § 4.2).

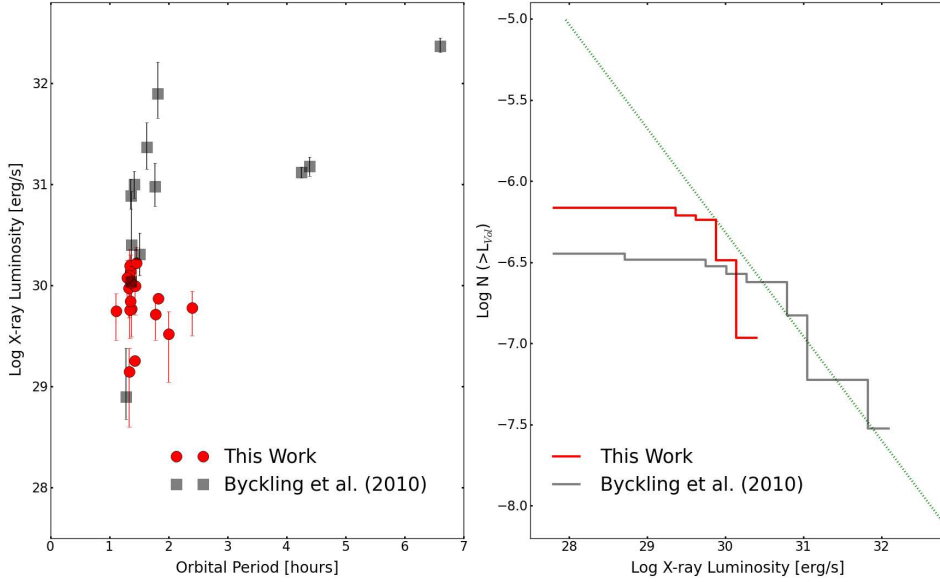


Figure 5. *Left:* X-ray luminosity (0.5–10 keV) versus orbital periods for the sample presented in this work (red) and that of Byckling et al. (2010, their Fig. 7) (black). The 2–10 keV flux quoted in the latter was converted to the 0.5–10 keV range using the model detailed in Table 2. *Right:* Cumulative source distribution as a function of X-ray luminosity for our sample (red) and for that presented in Byckling et al. (2010, their Fig. 6) (black). The dashed line shows the powerlaw $N(> L) = k(L/L_t)^{-\alpha}$, where $k = 2.39 \times 10^{-7} \text{ pc}^{-3}$ and $L_t = 3 \times 10^{30} \text{ erg s}^{-1}$ as per Byckling et al. (2010).

5 DISCUSSION

Suggestions that the Galactic ridge X-ray emission is diffuse came about due to failure in fully resolving the emission into point sources (e.g. Ebisawa et al. 2001). Non-magnetic CVs have also been dismissed as a main contributor to the GRXE (e.g. Sazonov et al. 2006; Revnivtsev et al. 2006b) due to suggestions that the overall population is too luminous, with a mean X-ray luminosity greater than $\sim 10^{31} \text{ erg s}^{-1}$ (e.g. Eracleous et al. 1991; Richman 1996; Verbunt et al. 1997; Baskill et al. 2005). We argue here that the latter is likely a result of a selection bias in their X-ray luminosity function caused by the predominant use of X-ray selected samples. By studying an optically-selected sample of non-magnetic, intrinsically faint CVs, we find a population of low X-ray luminosity CVs, having an average luminosity of $\langle L_{0.5-10} \rangle = 8 \times 10^{29} \text{ erg s}^{-1}$ which still resembles the X-ray spectrum of the Galactic Ridge. This population, if found to exist in large numbers, could be a strong contributor to the overall GRXE below $\sim 10 \text{ keV}$.

The X-ray spectra of CVs are often characterised by a two-temperature plasma model (see e.g. Mukai & Shiokawa 1993; Baskill et al. 2005). In Sect. 4.2 we showed that the combined spectrum of this sample of twenty low-luminosity CVs has the same spectral characteristics as that of the better known, high-luminosity CVs (Fig. 2). This two-temperature spectrum closely resembles that of the Galactic ridge X-ray emission (Mukai & Shiokawa 1993). Eighteen out of the twenty sources in our sample were detected with Swift XRT and were found to have X-ray luminosities in the range $10^{28-30} \text{ erg s}^{-1}$. Figure 4 shows this distribution together with the upper limit of the two sources having a count rate consistent with zero. The peak of the distribution for the optically-selected sample used here is considerably lower than that presented by Verbunt et al. (1997) of $\langle \log(L_{2.0-10}) \rangle = 30.8$ (shown in green in Fig. 4), especially after considering the larger energy range used here (Fig. 3). This difference is clearly a result of the different biases in the selection of the two samples.

Byckling et al. (2010) presented a thorough analysis of the

X-ray luminosity function in an optically-selected sample of CVs having parallax-based distance measurements. In that study, the authors find a peak in the luminosity function at $\sim 10^{30-31} \text{ erg s}^{-1}$, systematically lower than previous – X-ray selected – studies but still more luminous than the result found here. Figure 5 (*left*) shows the Byckling et al. (2010) sample (black) together with our results (red) for the Luminosity–Orbital period plane. It is clear that we are probing a different parameter space to Byckling et al. (2010), with overall low orbital periods as expected for more evolved, and thus intrinsically fainter, systems. We also show in Fig. 5 (*right*) the cumulative distribution – $\text{Log } N(> L_{\text{Vol}})$ where L_{Vol} is the luminosity per cubic parsec volume as a function of $\text{Log } L$. For the sample of Byckling et al. (2010), we assume a volume out to 200 pc, in accordance to the previous authors. For the sample presented here, the furthest object is located $\sim 400 \text{ pc}$ away (Table 2). However, as our sample is not complete out to this radius, we estimate a correction factor by noting that SDSS covered $8,000 \text{ deg}^2$ ($\sim 20\%$; see §2) of the sky and our sample uses 16 out of the 30 low luminosity systems detected in DR5. As the size of the population presented here is still highly uncertain, the normalisation of the $\log N$ – $\log S$ plot, and with it the space density of these systems, should be interpreted with extreme caution. Nonetheless, these results show that the sample presented in this work fills the gap between the only low-luminosity outlier (GW Lib at $L_{2-10} \sim 5 \times 10^{28} \text{ erg s}^{-1}$) in the sample of Byckling et al. (2010), and the peak of their distribution at $\sim 10^{30-31} \text{ erg s}^{-1}$.

It was shown by Pretorius et al. (2007) and Pretorius & Knigge (2012) that the vast majority of CVs could be fainter than $\sim 5 \times 10^{29} \text{ erg s}^{-1}$ – and thus yet undetected – based on the limits to their CV space density as found from *ROSAT* surveys. Munro et al. (2004) showed that to account for the diffuse emission within 20 pc of the Galactic centre, approximately 0.2% of stellar mass would have to be hard X-ray sources with $L_x > 3 \times 10^{29} \text{ erg s}^{-1}$. The total stellar mass within 20 pc of the Galaxy centre is estimated as $\approx 10^8 M_\odot$ (Launhardt et al. 2002) and hence $\approx 2 \times 10^5$ sources would be needed in that region. This is equivalent to a source den-

sity of $\sim 6 \text{ pc}^{-3}$ assuming a spherical region of radius 20 pc. By scaling according to the mass model of Launhardt et al. (2002) with a stellar density in the inner 20 pc of $1000 \text{ M}_{\odot} \text{ pc}^{-3}$ and a local stellar density of $0.1 \text{ M}_{\odot} \text{ pc}^{-3}$ the source density in the 20 pc region corresponds to a local density of $\approx 6 \times 10^{-4} \text{ pc}^{-3}$, which is significantly higher than that found in most current observational campaigns. However, population synthesis based on the standard CV evolution scenario indeed predict space densities which are larger than the current observed values, ranging from $\sim 10^{-5} \text{ pc}^{-3}$ (Politano 1996) to a few $\sim 10^{-4} \text{ pc}^{-3}$ (de Kool 1992). These models further predict that the population should be dominated by short period systems (see e.g. Kolb 1993; Kolb & Stehle 1996), similar to the population presented in this work (see Fig. 5). Interestingly, the upper limit on low-luminosity CVs – the undetected population in Pretorius & Knigge (2012) – does indeed add further empirical credence to population syntheses models (see Fig. 4 of Pretorius & Knigge 2012). If population syntheses models are correct then the population density for CVs should be greater than observed, and CVs having luminosities of a few $10^{29} \text{ erg s}^{-1}$ could thus be a major contributor to the GRXE.

It is now established that intermediate polars (IP) are important contributor to the GRXE above $L_{\text{x}} \sim 10^{30} \text{ erg s}^{-1}$ (e.g. Hong 2012, and references therein). However, IPs are both theoretically and empirically known to belong to the brightest and rarest end of the CV population. In a volume limited sample, IPs represent at best a few per cent the entire CV population (Downes et al. 2001, 2006).

6 CONCLUSIONS

Using *Swift*-XRT, a sample of twenty optically selected, non-magnetic CVs were observed and their X-ray luminosities (0.5–10.0 keV) determined. The sources luminosities were found to range between 10^{28} to $10^{31} \text{ erg s}^{-1}$ with an average value of $8 \times 10^{29} \text{ erg s}^{-1}$. Cataclysmic variables towards the low luminosity range would not have been detected by the various *Chandra* surveys of the Galactic centre, where their limiting sensitivity is $L_{0.5-7\text{keV}} \sim 10^{30} \text{ erg s}^{-1}$ at a distance of 8 kpc (Revnivtsev et al. 2009). Spectral analyses were made of the average co-added spectrum. The result is consistent with a two-temperature plasma at $\sim 0.6 \text{ keV}$ and $\sim 8 \text{ keV}$, similarly to that of the well studied high-luminosity population. The similarity between the spectra of the point sources and that of the GRXE suggests that this emission could indeed be produced by CVs. The present work demonstrates the use of optical selection in order to remove X-ray luminosity bias in CVs. The study of a larger optically selected sample would be advantageous in better understanding the luminosity function of CVs, however in order to determine the absolute contribution of CVs towards the GRXE one also needs to determine the corresponding population density function.

ACKNOWLEDGEMENTS

RCR thanks the Michigan Society of Fellows and NASA. RCR is supported by NASA through the Einstein Fellowship Program, grant number PF1-120087 and is a member of the Michigan Society of Fellows. PJW and BTG acknowledge support from the UK STFC in the form of a Rolling Grant. JPO acknowledges the support of the UK Space Agency. This work also made use of data supplied by the UK Swift Science Data Centre at the University of Leicester. We also thank the anonymous referee for his/her constructive comments.

REFERENCES

- Adelman-McCarthy J. K., Agüeros M. A., Allam S. S., et al., 2006, *ApJS*, 162, 38
- Anders E., Grevesse N., 1989, *Geochimica et Cosmochimica Acta*, 53, 197
- Araujo-Betancor S., Gänsicke B. T., Hagen H., et al., 2005, *A&A*, 430, 629
- Arnaud K. A., 1996, in *Astronomical Data Analysis Software and Systems V*, edited by G. H. Jacoby & J. Barnes, vol. 101 of *Astronomical Society of the Pacific Conference Series*, 17–
- Balucinska-Church M., McCammon D., 1992, *ApJ*, 400, 699
- Baskill D. S., Wheatley P. J., Osborne J. P., 2005, *MNRAS*, 357, 626
- Beuermann K., Baraffe I., Kolb U., Weichhold M., 1998, *A&A*, 339, 518
- Boyd D., Oksanen A., Henden A., 2006, *Journal of the British Astronomical Association*, 116, 187
- Byckling K., Mukai K., Thorstensen J. R., Osborne J. P., 2010, *MNRAS*, 408, 2298
- Cash W., 1979, *ApJ*, 228, 939
- Cooke B. A., Griffiths R. E., Pounds K. A., 1970, in *Non-Solar X- and Gamma-Ray Astronomy*, edited by L. Gratton, vol. 37 of *IAU Symposium*, 280–
- Copperwheat C. M., Marsh T. R., Dhillon V. S., et al., 2009, *MNRAS*, 393, 157
- de Kool M., 1992, *A&A*, 261, 188
- Dillon M., Gänsicke B. T., Aungwerojwit A., et al., 2008, *MNRAS*, 386, 1568
- Dogiel V. A., Inoue H., Masai K., Schönfelder V., Strong A. W., 2002, *ApJ*, 581, 1061
- Downes R. A., Webbink R. F., Shara M. M., Ritter H., Kolb U., Duerbeck H. W., 2001, *PASP*, 113, 764
- Downes R. A., Webbink R. F., Shara M. M., Ritter H., Kolb U., Duerbeck H. W., 2006, *VizieR Online Data Catalog*, 5123, 0
- Draper A. R., Ballantyne D. R., 2009, *ApJ*, 707, 778
- Ebisawa K., Maeda Y., Kaneda H., Yamauchi S., 2001, *Science*, 293, 1633
- Eracleous M., Halpern J., Patterson J., 1991, *ApJ*, 382, 290
- Gänsicke B. T., Beuermann K., Thomas H., 1997, *MNRAS*, 289, 388
- Gänsicke B. T., Dillon M., Southworth J., et al., 2009, *MNRAS*, 397, 2170
- Gänsicke B. T., Hagen H., Engels D., 2002, in *The Physics of Cataclysmic Variables and Related Objects*, edited by B. T. Gänsicke, K. Beuermann, & K. Reinsch, vol. 261 of *Astronomical Society of the Pacific Conference Series*, 190–
- Gänsicke B. T., Long K. S., Barstow M. A., Hubeny I., 2006a, *ApJ*, 639, 1039
- Gänsicke B. T., Marsh T. R., Edge A., et al., 2005a, *MNRAS*, 361, 141
- Gänsicke B. T., Rodríguez-Gil P., Marsh T. R., et al., 2006b, *MNRAS*, 365, 969
- Gänsicke B. T., Sion E. M., Beuermann K., Fabian D., Cheng F. H., Krautter J., 1999, *A&A*, 347, 178
- Gänsicke B. T., Szkody P., Howell S. B., Sion E. M., 2005b, *ApJ*, 629, 451
- Gehrels N., Chincarini G., Giommi P., et al., 2004, *ApJ*, 611, 1005
- Giacconi R., Gursky H., Paolini F. R., Rossi B. B., 1962, *Physical Review Letters*, 9, 439
- Hamada T., Salpeter E. E., 1961, *ApJ*, 134, 683
- Hong J., 2012, *ArXiv e-prints*

- Howell S. B., Gänsicke B. T., Szkody P., Sion E. M., 2002, *ApJ*, 575, 419
- Howell S. B., Nelson L. A., Rappaport S., 2001, *ApJ*, 550, 897
- Ishioaka R., Sekiguchi K., Maehara H., 2007, *PASJ*, 59, 929
- Kaneda H., Makishima K., Yamauchi S., Koyama K., Matsuzaki K., Yamasaki N. Y., 1997, *ApJ*, 491, 638
- Kato T., Nogami D., Matsumoto K., Baba H., 2004, *PASJ*, 56, 109
- Kirkpatrick J. D., Reid I. N., Liebert J., et al., 1999, *ApJ*, 519, 802
- Kirkpatrick J. D., Reid I. N., Liebert J., et al., 2000, *AJ*, 120, 447
- Kolb U., 1993, *A&A*, 271, 149
- Kolb U., Stehle R., 1996, *MNRAS*, 282, 1454
- Koyama K., Maeda Y., Sonobe T., Takeshima T., Tanaka Y., Yamauchi S., 1996, *PASJ*, 48, 249
- Koyama K., Makishima K., Tanaka Y., Tsunemi H., 1986, *PASJ*, 38, 121
- Lanz T., Hubeny I., 1995, *ApJ*, 439, 905
- Launhardt R., Zylka R., Mezger P. G., 2002, *A&A*, 384, 112
- Liedahl D. A., Osterheld A. L., Goldstein W. H., 1995, *ApJ*, 438, L115
- Littlefair S. P., Dhillon V. S., Marsh T. R., et al., 2008, *MNRAS*, 388, 1582
- Littlefair S. P., Dhillon V. S., Marsh T. R., Gänsicke B. T., 2006a, *MNRAS*, 371, 1435
- Littlefair S. P., Dhillon V. S., Marsh T. R., Gänsicke B. T., Baraffe I., Watson C. A., 2007, *MNRAS*, 381, 827
- Littlefair S. P., Dhillon V. S., Marsh T. R., Gänsicke B. T., Southworth J., Watson C. A., 2006b, *Science*, 314, 1578
- Mewe R., Lemen J. R., van den Oord G. H. J., 1986, *A&AS*, 65, 511
- Moretti A., Pagani C., Cusumano G., et al., 2009, *A&A*, 493, 501
- Mukai K., Kinkhabwala A., Peterson J. R., Kahn S. M., Paerels F., 2003, *ApJ*, 586, L77
- Mukai K., Shiokawa K., 1993, *ApJ*, 418, 863
- Muno M. P., Baganoff F. K., Bautz M. W., et al., 2004, *ApJ*, 613, 326
- Murakami H., Koyama K., Sakano M., Tsujimoto M., Maeda Y., 2000, *ApJ*, 534, 283
- Patterson J., Kemp J., Skillman D. R., et al., 1998, *PASP*, 110, 1290
- Patterson J., Thorstensen J. R., Armstrong E., Henden A. A., Hynes R. I., 2005a, *PASP*, 117, 922
- Patterson J., Thorstensen J. R., Armstrong E., Henden A. A., Hynes R. I., 2005b, *PASP*, 117, 922
- Patterson J., Thorstensen J. R., Kemp J., 2005c, *PASP*, 117, 427
- Patterson J., Thorstensen J. R., Kemp J., 2005d, *PASP*, 117, 427
- Patterson J., Thorstensen J. R., Kemp J., et al., 2003, *PASP*, 115, 1308
- Patterson J., Thorstensen J. R., Knigge C., 2008, *PASP*, 120, 510
- Politano M., 1996, *ApJ*, 465, 338
- Pretorius M. L., Knigge C., 2012, *MNRAS*, 419, 1442
- Pretorius M. L., Knigge C., O'Donoghue D., Henry J. P., Gioia I. M., Mullis C. R., 2007, *MNRAS*, 382, 1279
- Pretorius M. L., Woudt P. A., Warner B., Bolt G., Patterson J., Armstrong E., 2004, *MNRAS*, 352, 1056
- Revnivtsev M., Molkov S., Sazonov S., 2006a, *MNRAS*, 373, L11
- Revnivtsev M., Sazonov S., Churazov E., Forman W., Vikhlinin A., Sunyaev R., 2009, *Nat*, 458, 1142
- Revnivtsev M., Sazonov S., Gilfanov M., Churazov E., Sunyaev R., 2006b, *A&A*, 452, 169
- Revnivtsev M., Sazonov S., Sunyaev R., 2007, *Progress of Theoretical Physics Supplement*, 169, 125
- Richman H. R., 1996, *ApJ*, 462, 404
- Sazonov S., Revnivtsev M., Gilfanov M., Churazov E., Sunyaev R., 2006, *A&A*, 450, 117
- Schwarz G. J., Barman T., Silvestri N., et al., 2004, *PASP*, 116, 1111
- Southworth J., Marsh T. R., Gänsicke B. T., et al., 2007, *MNRAS*, 382, 1145
- Stoughton C., Lupton R. H., Bernardi M., et al., 2002, *AJ*, 123, 485
- Szkody P., Anderson S. F., Brooks K., et al., 2011, *AJ*, 142, 181
- Szkody P., Anderson S. F., Hayden M., et al., 2009, *AJ*, 137, 4011
- Szkody P., Gänsicke B. T., Sion E. M., Howell S. B., 2002, *ApJ*, 574, 950
- Tammann G. A., 1982, in *NATO ASIC Proc. 90: Supernovae: A Survey of Current Research*, edited by M. J. Rees & R. J. Stoneham, 371–403
- Tanaka Y., Miyaji T., Hasinger G., 1999, *Astronomische Nachrichten*, 320, 181
- Templeton M. R., Leaman R., Szkody P., et al., 2006, *PASP*, 118, 236
- Townsley D. M., Bildsten L., 2003, *ApJ*, 596, L227
- Townsley D. M., Gänsicke B. T., 2009, *ApJ*, 693, 1007
- Uthas H., Knigge C., Long K. S., Patterson J., Thorstensen J., 2011, *MNRAS*, 414, L85
- Uthas H., Patterson J., Kemp J., et al., 2012, *MNRAS*, 420, 379
- van Teeseling A., Verbunt F., 1994, *A&A*, 292, 519
- Vanlandingham K. M., Schwarz G. J., Howell S. B., 2005, *PASP*, 117, 928
- Verbunt F., Bunk W. H., Ritter H., Pfeiffermann E., 1997, *A&A*, 327, 602
- Warwick R. S., Norton A. J., Turner M. J. L., Watson M. G., Willingale R., 1988, *MNRAS*, 232, 551
- Warwick R. S., Pérez-Ramírez D., Byckling K., 2011, *MNRAS*, 413, 595
- Warwick R. S., Turner M. J. L., Watson M. G., Willingale R., 1985, *Nat*, 317, 218
- Watson M. G., Marsh T. R., Fender R. P., et al., 1996, *MNRAS*, 281, 1016
- Wheatley P. J., Burleigh M. R., Watson M. G., 2000a, *MNRAS*, 317, 343
- Wheatley P. J., Burleigh M. R., Watson M. G., 2000b, *MNRAS*, 317, 343
- Wheatley P. J., Verbunt F., Belloni T., et al., 1996, *A&A*, 307, 137
- Worrall D. M., Marshall F. E., Boldt E. A., Swank J. H., 1982, *ApJ*, 255, 111
- Woudt P. A., Warner B., 2004, *MNRAS*, 348, 599
- Woudt P. A., Warner B., Pretorius M. L., 2004, *MNRAS*, 351, 1015
- Woudt P. A., Warner B., Pretorius M. L., Dale D., 2005, in *The Astrophysics of Cataclysmic Variables and Related Objects*, edited by J.-M. Hameury & J.-P. Lasota, vol. 330 of *Astronomical Society of the Pacific Conference Series*, 325–+
- Yamauchi S., Kaneda H., Koyama K., et al., 1996, *PASJ*, 48, L15
- York D. G., Adelman J., Anderson Jr. J. E., et al., 2000, *AJ*, 120, 1579
- Yuasa T., Makishima K., Nakazawa K., 2012, *ApJ*, 753, 129
- Yusef-Zadeh F., Law C., Wardle M., 2002, *ApJ*, 568, L121
- Zdziarski A. A., 1996, *MNRAS*, 281, L9
- Zharikov S. V., Tovmassian G. H., Napiwotzki R., Michel R., Neustroev V., 2006, *A&A*, 449, 645